Lamb wave defect detection and evaluation using a fully non-contact laser system

Zhaoyun Ma, Lingyu Yu

Department of Mechanical Engineering, University of South Carolina, Columbia, SC, 29208, USA

zhaoyun@email.edu , yu3@cec.sc.edu

ABSTRACT

Traditional Lamb wave structural health monitoring (SHM)/nondestructive evaluation (NDE) system employs contact type transducers such as PZT, ultrasonic transducers, and optical fibers. In application, transducer attachment and maintenance can be time and labor consuming. In addition, the use of couplant and adhesives can introduce additional materials on structures, and the interface coupling is often not well understood. To overcome these limitations, we proposed a fully non-contact NDE system by employing pulsed laser (PL) for Lamb wave actuation and scanning laser Doppler vibrometer (SLDV) for Lamb wave sensing. The proposed system is implemented on aluminum plates. The PL Lamb wave excitation is calibrated, and the optimal parameters are obtained. Lamb wave modes are then characterized through 1D wavefield analysis. With the calibrated and characterized system, defect detection and evaluation are achieved on aluminum plates with simulated defects (surfaced-bonded quartz rod, and machine milled crack) through 1D and 2D inspection in both time-space and frequency-wavenumber domains.

Keywords: Lamb waves, non-contact inspection, pulsed laser, laser vibrometer

1 INTRODUCTION

Structural health monitoring (SHM) and nondestructive evaluation (NDE) have been successfully applied in structural design and maintenance in aerospace, civil, and nuclear engineering [1]-[5]. Among various SHM/NDE methods, Lamb wave ultrasonic methods have drawn researcher's attention since they can propagate long distance with less energy loss [2][5] and they are sensitive to various defects [1][5][6]. Various transducers have been employed for Lamb wave actuation such as lead zirconate titanate transducers (PZT) [7][8], pulsed laser [9]-[13], air-coupled transducers (ACT) [14][15]; and for Lamb wave sensing, PZT [7], ACT [15], electromagnetic acoustic transducers (EMAT) [16][17], laser Doppler vibrometer [18]-[20], and optical fibers [21][22] have all been reported.

Based on the way the transducers/sensors are installed on host structure, Lamb wave transducers/sensors can be categorized into contact and non-contact types. Contact type transducers are normally attached on the surface of the host structure using couplant or bonding adhesives. They are used more often and have been demonstrated extensively in literature [5]-[8]. However, the use of couplant or adhesives introduces additional materials onto structures and exact mechanisms of interfacing are often not completely understood. In addition, it is difficult to perform inspection with contact NDE system for structures in certain conditions such as hot surfaces. Thus, it is important to develop a fully non-contact NDE system that can

overcome these limitations. For non-contact sensing, scanning Laser Doppler vibrometer (SLDV) has been adopted in Lamb wave applications to provide multidimensional sensing in recent years [18]-[20]. The SLDV operates on Doppler effect and can measure the particle motions along the laser beam. The scanning capability of SLDV allows for acquisition of Lamb wavefields along both time and space dimension such that wavenumber information can be derived through multidimensional Fourier analysis [23]. For non-contact Lamb wave actuation, ACT [14][15], EMAT [16][17] and pulsed laser [9]-[13] have been used. Among them pulsed laser has the advantages of achieving non-contact actuation at a relative far distance and being applicable to both metals and composites [10]-[13]. When operating in the thermoelastic region, the pulsed laser is considered to provide a nondestructive means for Lamb wave actuation [9][12].

In this paper, a non-contact PL-SLDV laser system is proposed and evaluated for defect inspection in aluminum plates. To actuate Lamb waves for effective SHM/NDE, the PL for Lamb wave excitation is studied and characterized experimentally, and optimal parameters on a 1 mm thick aluminum plate are determined. After PL-SLDV laser system is configured, Lamb wave characterization is further performed through examination in both time-space and frequency-wavenumber domains. Finally, toward applications for SHM/NDE, 1D and 2D Lamb wave inspection on aluminum plates with simulated defects (surfaced-bonded quartz and milled crack) are conducted. Damage detection based on multidimensional Lamb wave analysis are carried out. The development of the non-contact PL-SLDV system combined with effective defect evaluation is believed to enable rapid inspection and health monitoring methods toward new structural systems in the long run.

2   PL-SLDV SYSTEM CONFIGURATION

2.1 *PL-SLDV experimental setup*

The non-contact PL-SLDV system is configured in this section for Lamb wave inspection. A Q-switch pulsed laser (model: Quantel CFR400) with 1064 nm wavelength is selected as the actuator for the PL-SLDV system. The pulse width of the selected pulsed laser is 7 ns, and the near field beam diameter is 5.5-mm. The sensing system adopts SLDV (model: Polytec PSV-400) with sampling rate at 10.24 MHz and using velocity decoder VD-09 (maximum frequency 1MHz). The overall experimental setup is shown in Figure 1a. The PL and SLDV heads are placed on each side of the testing plate and both laser heads are set normal to the specimen. With such setup, SLDV measures the out-of-plane surface particle velocity of Lamb waves. Q-switch is used to send command to PL control box to enable the PL actuation and trigger the SLDV measurement simultaneously.

A 1-mm thick aluminum 2024-T3 plate (size: 610 mm × 610 mm × 1mm) is used for the PL-SLDV system configuration study. The schematic of PL actuation and SLDV sensing is illustrated in Figure 1b. Cartesian coordinate is set with PL actuation as its origin. The SLDV scanning is along *x* direction and set 20 mm away from the PL actuation point with a spatial resolution of 1 mm. Clay is added on the edge of the specimen to minimize boundary reflection. Reflective tape is put on the plate to improve the light reflection of the specimen surface to achieve high signal-to-noise ratio (SNR) for SLDV sensing.
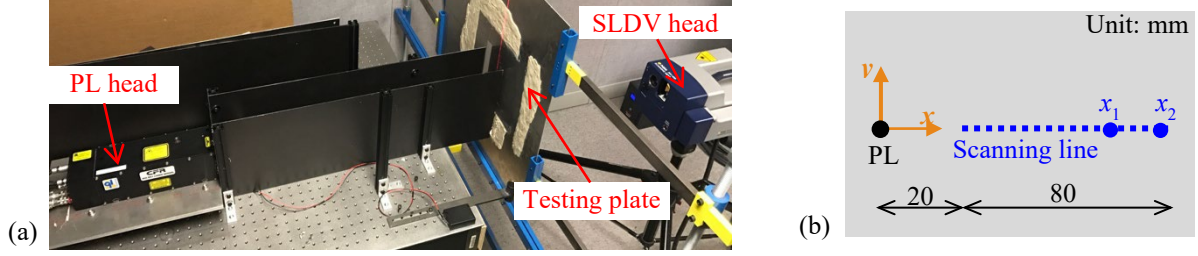
Figure 1   Non-contact PL-SLDV laser inspection system: (a) overall experimental setup, and (b) schematic of the actuation and sensing

2.2 PL-SLDV Lamb wave actuation and sensing

The Lamb wave excited in plate is known to be correlated with the input laser energy. Therefore, we first experimentally investigated the excitation energy for PL Lamb wave actuation. The waveforms at 60 mm away from the excitation point (x_1 in Figure 1b) are recorded with different excitation energy set at 3% to 100% of the full power (330 mJ per pulse). Selected waveforms and corresponding frequency spectrum (10%, 50% and 100%) are plotted in Figure 2. Under low excitation energy, e.g. 33 mJ, the waveforms are noisy and Lamb wave modes are difficult to observe. At high excitation energy, e.g. 166 mJ, Lamb wave modes become recognizable where a faster wave package with lower strength (black circle) and a slower one with higher strength (red circle) are observed. The SNR and bandwidth of full width at half maximum (FWHM) are calculated to characterize the signals. The SNR and bandwidth variation with excitation energy are plotted in Figure 3a and Figure 3b respectively. The bandwidth does not change significantly (around 70 kHz) while the SNR increases with the increase of excitation energy. When excitation energy is 100 mJ, the SNR is 10.27 dB, which is acceptable for further Lamb wave mode evaluation and damage detection.
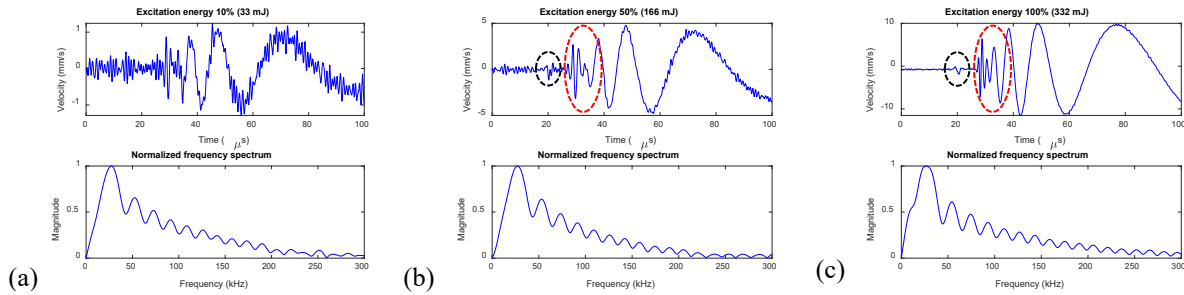

Figure 2   Waveforms at 60 mm and corresponding frequency spectrum at selected excitation energy: (a) 10%, (b) 50%, and (d) 100%, showing the SNR improves with excitation energy increase, while bandwidth does not change significantly

The average times are also calibrated in order to further improve SNR with low excitation energy (33 mJ). The waveforms at x_2 (Figure 1b, furthest scanning point) averaging from 1 to 8 times are recorded and plotted in Figure 3, showing that signal quality improves with the averaging times. With averaging 4 times, the SNR reaches 10.29 dB, which is acceptable for signal quality. Appropriate averaging times can be adjusted according to the inspection requirement in applications.
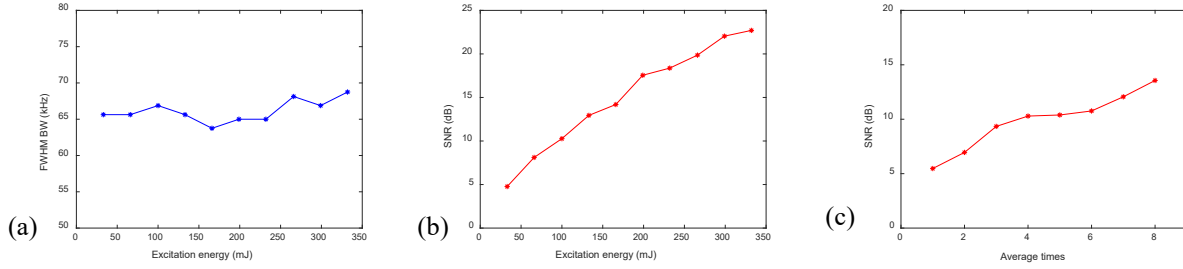
3

Figure 3   Signal evaluation through: (a) BW change with respect to (w.r.t.) excitation energy, (b) SNR change w.r.t. excitation energy, and (c) SNR change w.r.t. average times

2.3 *PL Lamb wave characterization*

Waveforms shown in Figure 2b and Figure 2c present a faster wave packet with lower strength and a slower one with much higher strength. From theoretical Lamb wave dispersion in the 1-mm aluminum plate [7], it is known they are the fundamental S0 and A0 Lamb wave mode, respectively. To confirm the presence of the Lamb wave modes, 1D wavefield is obtained through line scan for frequency-wavenumber (*f-k*) analysis [23]. The line scan setup is given in Figure 1b, which is along *x* direction with 1 mm spatial resolution. The PL excitation energy is set as 100 mJ, and 5 averages are used for the SLDV sensing to obtain more effective inspection information.

The time-space wavefield is plotted in Figure 4a. Faster S0 mode with weaker out-of-plane motion followed by slower A0 mode with stronger out-of-plane motion are observed. *f-k* analysis is performed for the recorded wavefield through 2D fast Fourier transform and the obtained *f-k* representation are plotted in Figure 4b. The results in the *f-k* domain show weak S0 and strong A0 in the frequency range 0-800 kHz, which are consistent with the time-space wavefield. Thus, with the PL-SLDV system, Lamb wave modes S0 and A0 are excited in the testing aluminum plate.
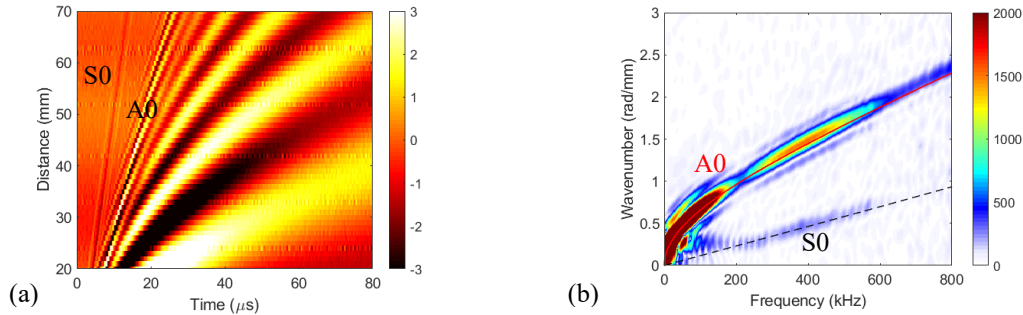

Figure 4   PL Lamb wave characterization: (a) time-space wavefield with excitation energy 100 mJ, and (b) frequency-wavenumber representation, showing that Lamb wave modes S0 and A0 are excited in the aluminum plate. Note: the red line is the theoretical A0 dispersion curve, and the black line is the theoretical S0 dispersion curve.

In the preliminary tests, surface burn is observed at high energy excitation: 40, 70 and 100 mJ. The surface burn is showing as whitish dust shown in Figure 5a. To avoid the surface burning, an 0.7-mm thick aluminum foil with 8-mm diameter is added at the excitation point surface. In

4

order to guarantee that comparable PL Lamb waves can be excited with this surface protection, Lamb wave characterization is performed through line scan (with the same set up for raw surface) for *f-k* analysis. The time-space wavefield along the scanning line and its *f-k* representation are plotted in Figure 5a and Figure 5b respectively. Weaker and faster S0 mode, and stronger and slower A0 mode are observed in both the wavefield and *f-k* spectrum. Thus, PL Lamb waves are successfully excited with the surface protection, and the excited PL Lamb waves are comparable to raw surface condition.
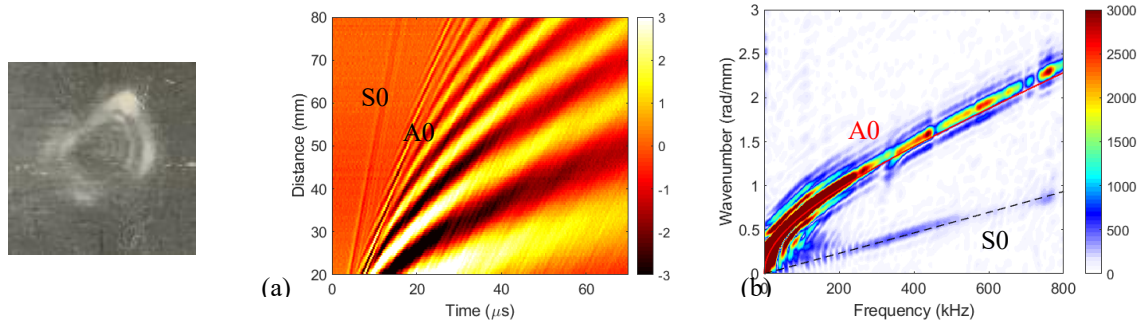

Figure 5   Surface protection evaluation: (a) surface burn with 100 mJ excitation energy, (b) time-space wavefield, and (c) *f-k* spectrum, showing that PL with surface protection achieved comparable Lamb wave actuation

3   DAMAGE INSPECTION ON AN ALUMINUM PLATE

With the demonstrated capability of PL Lamb wave actuation and optimal setup, this section focuses on application of the non-contact PL-SLDV system to inspect metallic plates with simulated defects (surfaced-bonded quartz rod and machine milled crack). Both line inspection and area inspection are performed on the damaged plates for defect detection and evaluation.

3.1 *Experimental setup*

Three 1-mm aluminum 2024-T3 plates are tested in the following experiments: one pristine plate, one damaged plate with surface bonded quartz rod shown in Figure 6a (10-mm thickness and 10-mm diameter), and one damaged plate with machine milled crack shown in Figure 6b (0.5-mm width and 10-mm length). The specimen schematic is shown in Figure 6c for 1D line inspection and Figure 6d for 2D area inspection with spatial resolution of 1 mm. Cartesian coordinates are used with excitation point set as origin and defects located at y=70 mm. The PL excitation energy is set as 100 mJ, and surface protection (0.7-mm thick aluminum foil) is attached at the origin. 10 averages are used in order to get a higher SNR for better inspection results.
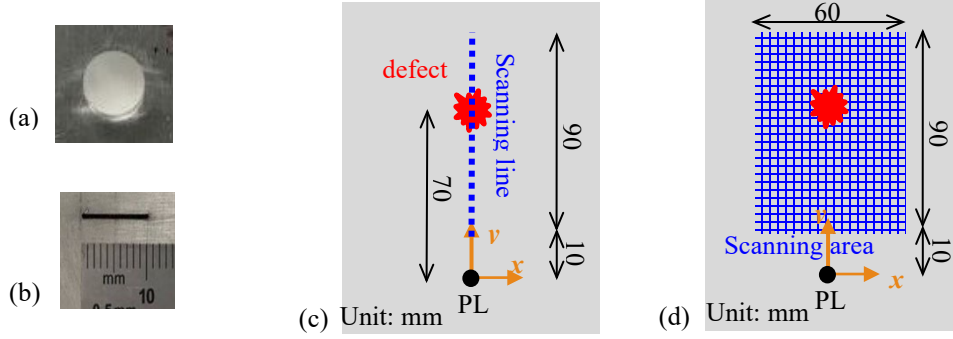
Figure 6   Schematic of specimen set up: (a) surface bonded quartz rod, (b) machine milled crack, (c) 1D line inspection set up, and (d) 2D area inspection setup

3.2 *1D line inspection results*

The acquired time-space wavefields along the scanning line are plotted in Figure 7a, b and c. Through 2D Fourier transform of the wavefield data, *f-k* spectra are obtained as shown in Figure 7d, e and f. For pristine plate, S0 and A0 Lamb wave modes are observed. The relative *f-k* spectrum (Figure 7d) is consistent with the wavefield result. The wavefield for quartz plate also shows that two incident wave modes S0 and A0. However, reflected waves appear at $x=65$ mm where the quartz edge is, and weak transmitted waves are observed after waves interacted with the quartz. In the corresponding *f-k* spectrum (Figure 7e), negative A0 is observed. The wavefield for crack plate also shows similar wave phenomenon as quartz plate. The difference is that the reflected waves are clearer, and the transmitted waves are stronger. In the corresponding *f-k* spectrum in Figure 7f, negative A0 is also observed as expected.

With 1D Lamb wave inspection, the quartz and crack are both detected and localized using wavefield analysis. However, the location of defects is not indicated in the *f-k* representations. Thus, short space-wavenumber (*x-k*) analysis is performed to further localize the defects and capture the wavenumber variation along the scanning line. 90 kHz is selected as the interested frequency since A0 is stronger at lower frequency. The calculated *x-k* spectrum at 90 kHz for the three plates are plotted in Figure 7g, h and i respectively. In the *x-k* spectrum of pristine plate (Figure 7g), only positive A0 is observed. Compared to pristine plate, negative A0 appears before $x=70$ mm for quartz plate (Figure 7h). This indicates that incident waves propagate and reflect after interacting with the quartz. After 70 mm, only weak positive A0 is observed, which is consistent with the relative wavefield where transmitted waves are relatively weak. In addition, new wavenumbers lower than A0 wavenumber (0.62 rad/mm) are observed. For crack plate, strong negative A0 is observed at the crack location ($x=70$ mm), while considerable waves transmitted after the crack as shown in Figure 7i. Moreover, new wavenumbers higher than A0 wavenumber are observed.
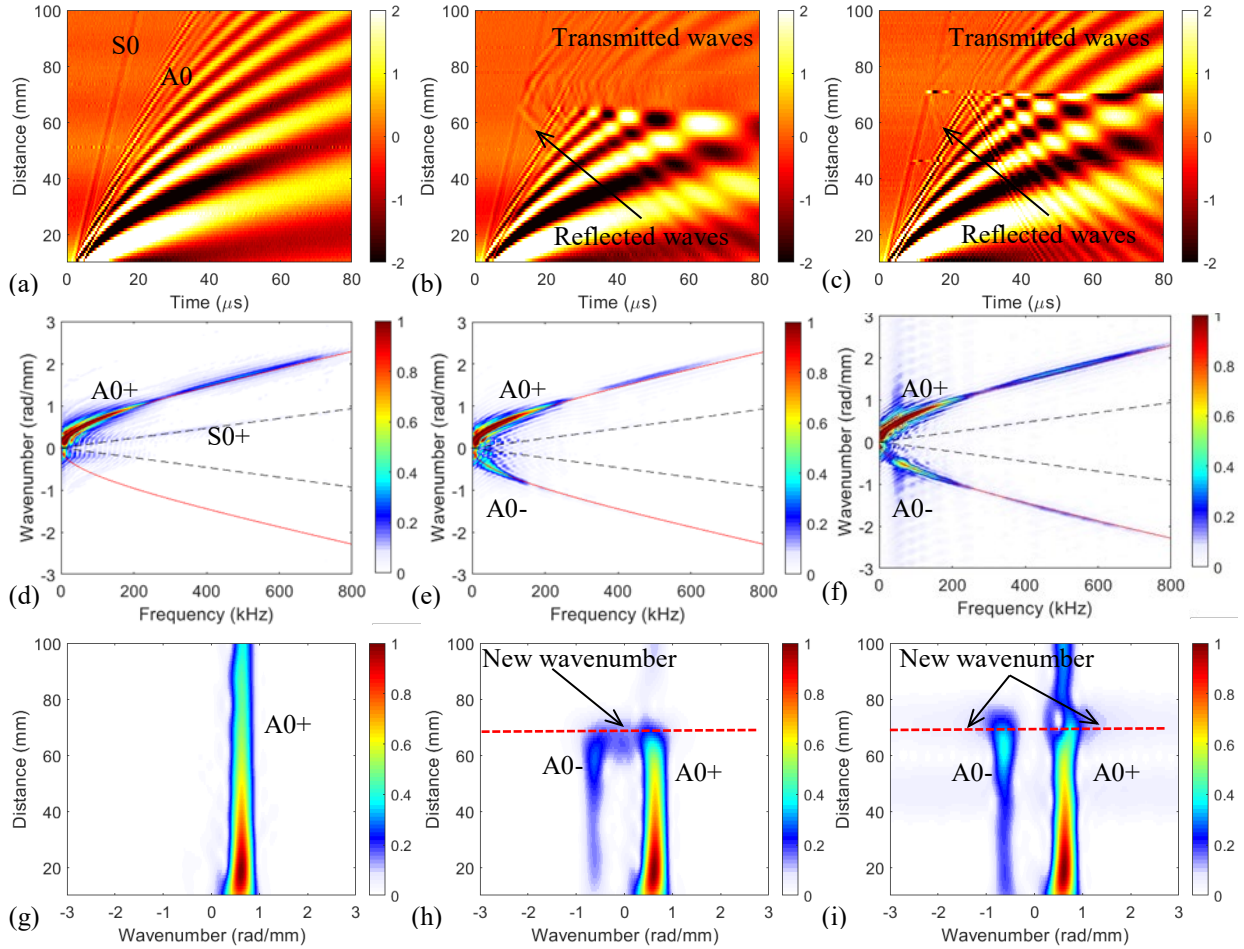
6

Figure 7   Time-space wavefields of: (a) pristine plate, (b) quartz plate, and (c) crack plate, showing Lamb wave interaction with different defects in each plate; frequency-wavenumber spectra of: (d) pristine plate, (e) quartz plate, and (f) crack plate, showing Lamb wave modes in frequency-wavenumber domain; short space-wavenumber spectra at 90 kHz of: (g) pristine plate, (h) quartz plate, and (i) crack plate, showing different wavenumber variation along the scanning line for each plate

3.3 *2D area inspection results*

In this section, 2D inspection and wavefield analysis are performed. The space wavefield at 17, 26 and 40 µs are captured and plotted in Figure 8 for each plate to show Lamb wave interaction with the selected defects. In Figure 8a, d and g, the 2D Lamb wave propagation in the pristine plate is illustrated, where the wave front is circular, and waves propagate smoothly along time. The 2D Lamb wave propagation in the quartz plate is shown in Figure 8b, e and h. At 17 µs, mode conversion from S0 to A0 is observed at *y*=70 mm (Figure 8b), and waves scattered since the quartz works as a new scatter source. After waves bypass the quartz, they split from around *y*=65 mm as shown in the wavefield at 40 µs (Figure 8h), resulting in that very little waves transmitted. For crack plate, weak reflective waves from S0 are observed at 17 µs (Figure 8c), while strong reflected waves from A0 are observed at 26 µs at *y*=70 mm. After that, waves

7

bypass the crack and transmitted waves are observed in the wavefield at 40 μs (Figure 8i). With the acquired time-space wavefields, the defects are localized at around 70 mm for both quartz and crack plates.
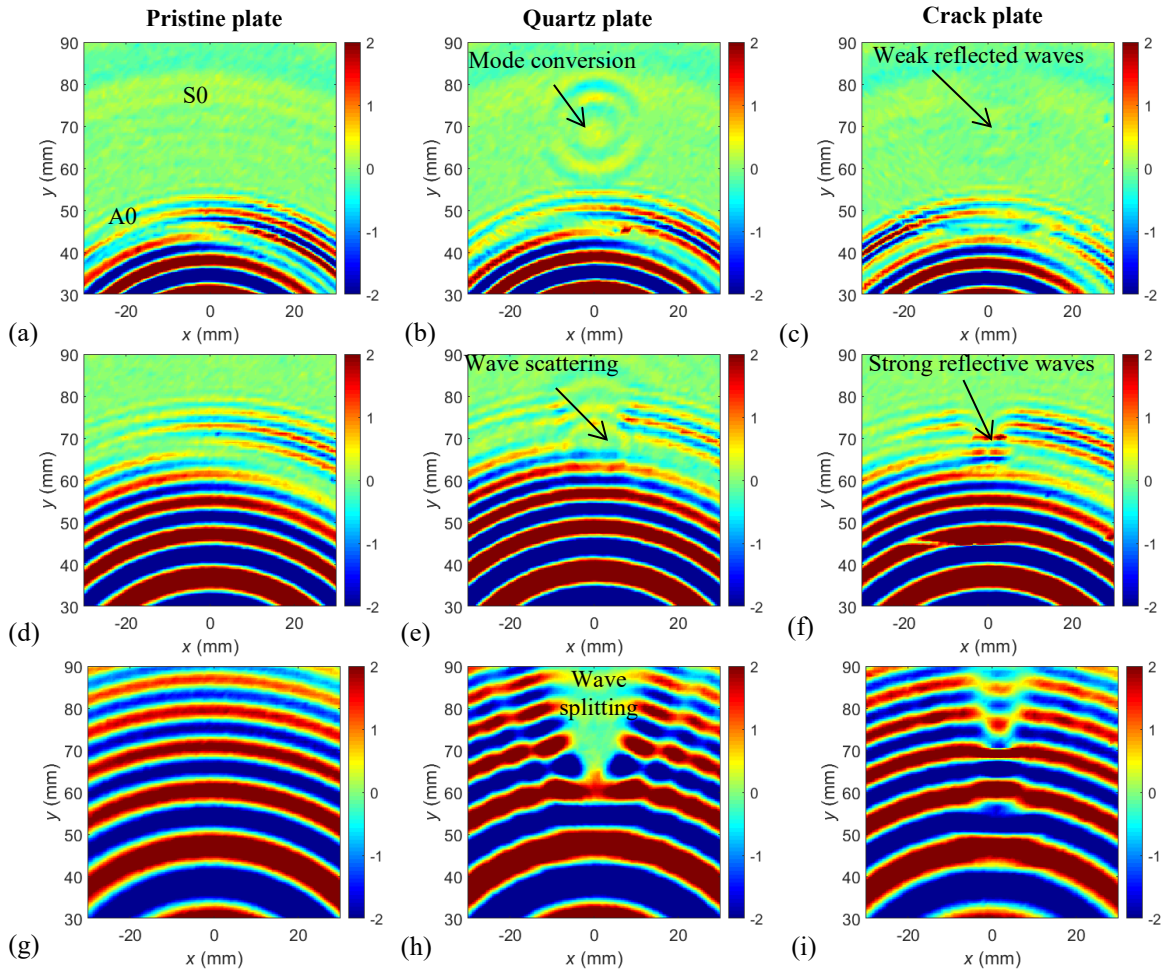

Figure 8   Wavefields at 17 μs for: (a) pristine plate, (b) quartz plate, and (c) crack plate; wavefields at 26 μs for: (d) pristine plate, (e) quartz plate, and (f) crack plate; wavefields at 40 μs for: (g) pristine plate, (h) quartz plate, and (i) crack plate, showing Lamb wave interaction with different defects differently

In order to observe the 2D inspection results in another perspective, the *f-k* analysis is performed through 3D Fourier transform. The obtained wavenumber spectrum at 90 kHz for pristine, quartz and crack plate are plotted in Figure 9a, b and c respectively. Since A0 is dominate at this interested frequency, only wavenumber changes related to A0 are discussed. In the wavenumber spectrum for pristine plate (Figure 9a), strong incident A0 is observed, which matches well with the theoretical A0 wavenumber curve (0.62 rad/mm). Compared to pristine condition, reflected A0 appears in the wavenumber spectrum for quartz and crack plate. In addition, new wavenumber components are observed: lower wavenumber components (<0.62 rad/mm) for quartz plate while high wavenumber components (> 0.62 rad/mm) for crack plate.
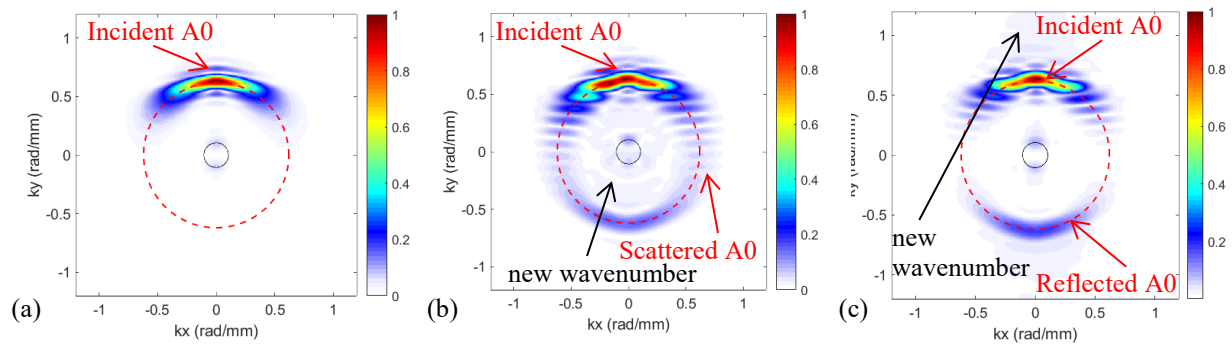
Figure 9   Wavenumber spectrum at 90 kHz for (a) pristine plate, (b) quartz plate, and (c) crack plate. Note: the red dash line is the theoretical A0 wavenumber curve at 90 kHz, and the black line is the theoretical S0 wavenumber curve at 90 kHz.

4   CONCLUSIONS

A fully non-contact PL-SLDV laser NDE system is proposed and configured. The PL excitation energy, and SLDV sensing average are studied on an aluminum plate in order to acquire signal with acceptable strength and SNR. In addition, the PL Lamb wave modes are characterized: faster and weaker S0, and stronger and slower A0 are excited. The configured PL-SLDV laser system is applied on aluminum plates with simulated defects (surface-boned quartz rod and milled crack). 1D line and 2D area inspection are performed, and PL Lamb wave signatures are captured when interacting with different defects: mode conversion dominates for quartz plate while reflection dominates for crack plate. Both defects are detected and localized through multidimensional Lamb wave analysis. Wavenumber changes are observed when Lamb waves interacting with different defects: except negative wavenumbers (A0-), higher wavenumbers (> 0.62 rad/mm) are observed for crack plate and lower wavenumbers are observed on quartz plate. With the proposed PL-SLDV system, future research will focus on surface protection development, analytical study of PL Lamb wave, imaging visualization of different defects, and implementation on composite plates.

5   ACKNOWLEDGEMENT

6   REFERENCES

[1]   Alleyne, D. N. and Cawley, P. (1992) "The Interaction of Lamb Waves with Defects," *Ieee* Transactions *on Ultrasonics Ferroelectrics and Frequency Control*, Vol. 39, pp. 381-397, 1992.

[2]   Rose, J. L. (1999) *Ultrasonic Waves in Solid Media*. Cambridge: Cambridge University Press, 1999.

[3]   Boller, C. (2000) "Next Generation Structural Health Monitoring and Its Integration into Aircraft Design," *International Journal of Systems Science*, Vol. 31, pp. 1333-1349, 2000.

[4]   Staszewski, W. J.; Boller, C. and Tomlinson, G. R. (2004) *Health Monitoring of Aerospace Structures*. Chichester: John Wiley & Sons, 2004.

[5]   Yu, L.; Leckey, C. A. and Tian, Z. (2013). "Study on crack scattering in aluminum plates with Lamb wave frequency-wavenumber analysis," *Smart Materials and Structures*, Vol. 22, No. 6, p. 065019, 2013.

[6]   Tian, Z.; Yu, L.; Leckey, C. and Seebo, J. (2015) "Guided wave imaging for detection and evaluation of impact-induced delamination in composites," *Smart Materials and Structures*, Vol. 24, No. 10, pp.105019, 2015.

[7]   Giurgiutiu, V. (2014) Structural Health Monitoring with Piezoelectric Wafer Active Sensors (Second Edition). Oxford: Academic Press, 2014.

[8]   Yu, L. and Tian, Z. (2013). "Lamb wave structural health monitoring using a hybrid PZT-laser vibrometer approach," *Structural Health Monitoring*, Vol.12, No. 5-6, 2013, pp. 469-483, 2013.

[9]   An, Y.K.; Park, B. and Sohn, H. (2013). "Complete noncontact laser ultrasonic imaging for automated crack visualization in a plate," *Smart Materials and Structures*, Vol. 22, No. 2, pp.025022, 2013.

[10]   Hess, P.; Lomonosov, A. M. and Mayer, A. P. (2014). "Laser-based linear and nonlinear guided elastic waves at surfaces (2D) and wedges (1D)," *Ultrasonics*, Vol. 54, No. 1, pp. 39-55, 2014.

[11]   Tan, Y.; Akhmadaliev, S.; Zhou, S.; Sun, S. and Chen, F. (2014). "Guided continuous-wave and graphene-based Q-switched lasers in carbon ion irradiated Nd: YAG ceramic channel waveguide," *Optics express*, Vol. 22, No. 3, pp. 3572-3577, 2014.

[12]   Tian, Z.; Howden, S.; Ma, Z.; Xiao, W. and Yu, L. (2019) "Pulsed laser-scanning laser Doppler vibrometer (PL-SLDV) phased arrays for damage detection in aluminum plates," Mechanical *Systems and Signal Processing*, Vol. 121, pp.158-170, 2019.

[13]   Toyama, N.; Ye, J.; Kokuyama, W. and Yashiro, S. (2019) "Non-Contact Ultrasonic Inspection of Impact Damage in Composite Laminates by Visualization of Lamb wave Propagation," *Applied Sciences*, Vol. 9, No. 1, pp. 46, 2019.

[14]   Castaings, M. and Cawley, P. (1996) "The generation, propagation, and detection of Lamb waves in plates using air-coupled ultrasonic transducers," *The Journal of the Acoustical Society of America*, Vol. 100, No. 5, pp.3070-3077.

[15]   Harb, M. S. and F. G. Yuan. (2016) "Non-contact ultrasonic technique for Lamb wave characterization in composite plates", *Ultrasonics*, Vol. 64, pp. 162-169, 2016.

[16]   Wilcox, P.D.; Lowe, M.J. and Cawley, P. (2005) "The excitation and detection of lamb waves with planar coil electromagnetic acoustic transducers," *IEEE Transactions on ultrasonics, ferroelectrics, and frequency control*, Vol. 52, No. 12, pp. 2370-2383, 2005.

[17]   Khalili, P. and Cawley, P. (2016) "Excitation of single-mode lamb waves at high-frequency-thickness products," *IEEE transactions on ultrasonics, ferroelectrics, and frequency control*, Vol. 63, No. 2, pp. 303-312, 2016.

[18]   Yu, L.; Tian, Z. and Leckey, C.A. (2015) "Crack imaging and quantification in aluminum plates with guided wave wavenumber analysis methods", *Ultrasonics*, Vol. 62, pp.203-212, 2015.

[19]   Staszewski W. J.; Lee B. C. and Traynor R. (2007) "Fatigue crack detection in metallic structures with Lamb waves and 3D laser vibrometry", *Meas Sci Technol*, Vol. 18, No. 3: pp. 727–739, (2007).

[20]   Tian, Z. and Yu, L. (2014). "Lamb wave frequency-wavenumber analysis and decomposition," *Journal of Intelligent Material Systems and Structures*, Vol.25, No. 9, pp. 1107-1123, 2014.

[21]   Betz, D.C.; Thursby, G.;Culshaw, B. and Staszewski, W.J. (2003) "Acousto-ultrasonic sensing using fiber Bragg gratings," *Smart Materials and Structures*, Vol. 12, No. 1, pp.122, 2003

[22]   Li F. C.; Murayama H. and Kageyama K., et al. (2009) "Guided wave and damage detection in composite laminates using different fiber optic sensors", *Sensors*, Vol. 9, No. 5: pp. 4005–4021, 2009.

[23]   Tian, Z. and Yu, L. (2014) "Lamb wave frequency–wavenumber analysis and decomposition," *Journal of Intelligent Material Systems and Structures*, Vol. 25, No. 9, pp.1107-1123, 2014.